

Self-Assembled Transparent Conductive Electrodes from Au Nanoparticles in Surfactant Monolayer Templates

Ahiud Morag, Liron Philosof-Mazor, Roman Volinsky, Elad Mentovich, Shachar Richter,* and Raz Jelinek*

Fabrication of thin, transparent conductive electrodes (TCEs) that are inexpensive, robust, and exhibit scalable surface areas is a highly sought after, though challenging, goal in optoelectronic, photovoltaic, and nanophotonics research and development.^[1,2] While most currently fabricated micro- and nanoelectronic devices are produced via top-down lithography methods,^[3] bottom-up approaches have emerged as promising alternatives for generation of organized nanostructures and electronic components.^[4] Bottom-up techniques generally rely upon molecular self-assembly phenomena to produce defined structures that could be practically utilized.^[5,6] Here, we describe a new bottom-up approach for construction of thin-film TCEs through self-assembly of alkyl-coated gold nanoparticles (Au NPs) within surfactant monolayer templates at the air/water interface. The Au nanostructures could be successfully transferred onto solid transparent surfaces; subsequent annealing and gold enhancement yielded a wide-area network of interconnected conductive Au nanowires. The thin-film electrodes exhibit high transparency, can be produced in varying length-scales and surface areas, and may be useful platforms for practical device applications.

Figure 1 depicts the experimental scheme. We begin with deposition at the air/water interface and isothermal compression of mixed monolayers composed of pentanethiol-coated Au NPs, elaidic acid, and myristyl alcohol (MOH; Figure 1a). Alkyl-coated Au NPs have been previously shown to form diverse 2D nanostructures on water surfaces through co-deposition of surfactant molecules or lipids.^[7–9] The two surfactant molecules employed here exhibit important roles: MOH forms condensed monolayer domains (green areas in Figure 1a).^[10] Elaidic acid, on the other hand, is capable of solubilizing Au NPs at the air/water interface in the temperature the experiments were carried out.^[5] Such

solubilization is important as it prevents formation of disordered Au NP aggregates, thus giving rise to a homogeneous distribution of Au NPs/elaidic acid mixture outside of the condensed MOH domains (grey areas in Figure 1a). Following isothermal compression of the tricomponent monolayer, the Au NPs are further constrained within narrow areas (Figure 1b) and finally transferred onto solid (transparent) substrates using a horizontal transfer (Langmuir–Schaefer method; Figure 1b). Efficient transfer is facilitated through pretreatment of the substrate surface with a hydrophobic coating (see Experimental Section).

The solid-supported Au NP film is further annealed in an argon environment at elevated temperature (around 350 °C) to remove the organic constituents, including both the alkyl capping layer coating the Au NPs and the surfactant molecules co-transferred from the air/water interface (Figure 1c). In a final stage, a gold seeding procedure^[11,12] based upon hydroquinone-reduction is carried out in which the film pattern acts as a surface scaffolding, designed to enhance and thicken the gold network (Figure 1d). Overall, the approach depicted in Figure 1 yields a transparent thin film composed of a continuous gold network that can be easily coupled to other device components.

Figure 2,3 show in situ and ex situ microscopy experiments that are aimed at characterizing the features and organization of the surfactant-patterned gold films. Figure 2 presents the surface pressure and area isotherm and the corresponding in situ Brewster angle microscopy (BAM)^[13] images recorded for the mixed monolayers. The BAM images presented in Figure 2a–c highlight the microscopic organization of the film components. Specifically, immediately following deposition of the Au NP/elaidic acid/MOH monolayer (Figure 2a) the rough contours of the condensed MOH domains appear (shown as dark islands) surrounded by the elaidic acid/Au NPs mixture (giving rise to the reflective, brighter areas in the monolayer due to the presence of the Au NPs). Further compression of the mixed monolayer to approximately 2 mN m^{−1} gave rise to a more visible localization of bright, homogeneous Au NP/elaidic acid regions around the condensed circularly shaped MOH domains (Figure 2b). The BAM images in Figure 2a and Figure 2b highlight the fundamental role of elaidic acid as a “2D solvent” for the Au NPs at the air/water interface.^[5] It should be emphasized that without co-deposition with elaidic acid, the Au NPs undergo significant aggregation at the temperature in which compression was carried out (data not shown). Figure 2c further shows that higher compression of the mixed monolayer (to approximately 12 mN m^{−1}) yielded an interconnected assembly of highly reflective regions containing Au NPs at the boundaries of hexagonal/circular MOH domains.

A. Morag, L. Philosof-Mazor, Prof. R. Jelinek
Department of Chemistry and Ilse Katz Institute for Nanotechnology
Ben Gurion University of the Negev
Beer Sheva 84105, Israel
E-mail: razj@bgu.ac.il

Dr. R. Volinsky
Helsinki Biophysics and Biomembrane Group
Faculty of Medicine
University of Helsinki
Helsinki, Finland

E. Mentovich, Dr. S. Richter
School of Chemistry
Tel Aviv University
Tel Aviv 69978, Israel
E-mail: srichter@post.tau.ac.il

DOI: 10.1002/adma.201101290

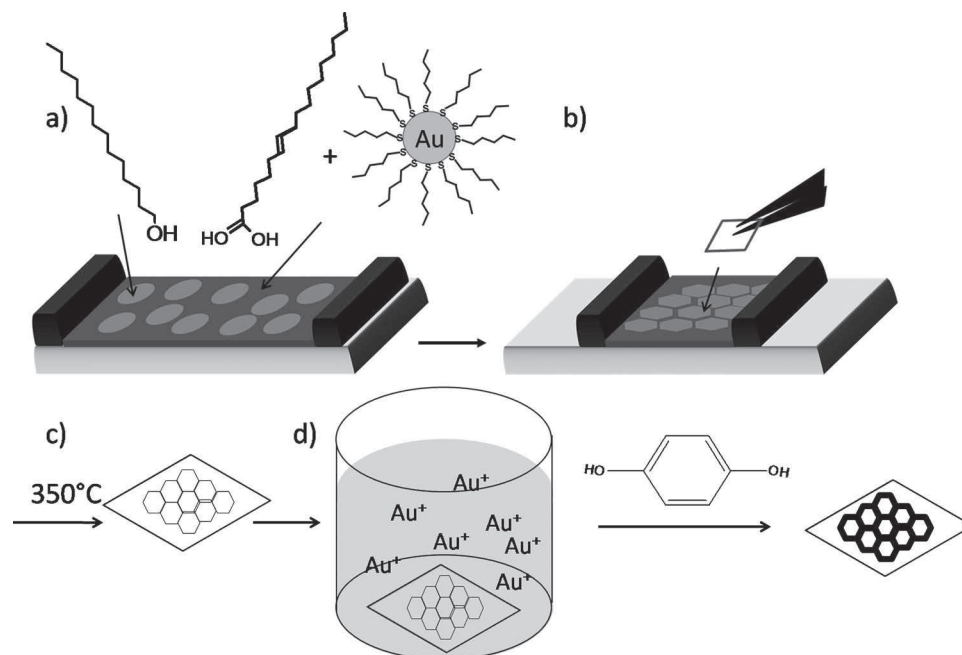


Figure 1. Experimental scheme (not to scale). a) Deposition of a Langmuir monolayer composed of myristoyl-alcohol (light grey domains), elaidic acid, and alkyl-capped Au NPs (dark grey areas). The blue base corresponds to water. b) The monolayer is isothermally compressed and subsequently transferred onto a solid substrate using the Langmuir-Schaefer method. c) Removal of organic substances through high-temperature annealing. d) Enhancement of the gold features using a hydroquinone-induced gold reduction procedure.

Following compression of the monolayer to a surface pressure of 12 mN m^{-1} , the surfactant-templated gold pattern was transferred using the Langmuir-Schaefer horizontal method onto a solid substrate precoated with a hydrophobic silane layer. Figure 3a shows a representative scanning electron microscopy (SEM) image of an elongated gold nanowire transferred onto the substrate from the air/water interface. The SEM image in Figure 3a highlights the remarkable order and uniformity of the

nanowire. The transmission electron microscopy (TEM) image in Figure 3b clearly shows that the gold nanowire is essentially composed of individual Au NPs transferred from the water surface. The TEM result in Figure 3b also points to the occurrence of discontinuities within the nanowire due to the alkyl layer surrounding the Au NPs.

To overcome the discontinuities in the nanowire and thus achieve effective electrical conductivity we further applied high-temperature annealing at around 350°C in an inert (argon) environment designed to remove all organic substances (both alkyl layer coating the Au NPs as well as surfactant molecules that make up the monolayer template) followed by a gold enhancement procedure.^[11,12] The enhancement process (also denoted as “gold seeding”) relied on soluble hydroquinone as the reducing agent and utilized the surface-deposited Au NP network as a scaffold catalyst for docking additional gold layers. Figure 3c features a SEM image of a nanowire fragment after annealing and gold enhancement. The SEM image in Figure 3c demonstrates that the ordered, relatively uniform wire structure was retained. In particular, the SEM analysis indicates that the discontinuities, which were apparent in the gold nanowire prior to gold enhancement (Figure 3a), were essentially “plugged”, yielding a much thicker, solid gold nanowire that retained the overall alignment (Figure 3c).

The wide-area gold nanowire pattern obtained following annealing and gold enhancement is shown in Figure 3d (SEM) and Figure 3e (optical microscopy). Both the SEM and optical microscopy images highlight the appearance of a continuous gold nanowire pattern on the transparent substrate covering a large surface area. The film organization depicted

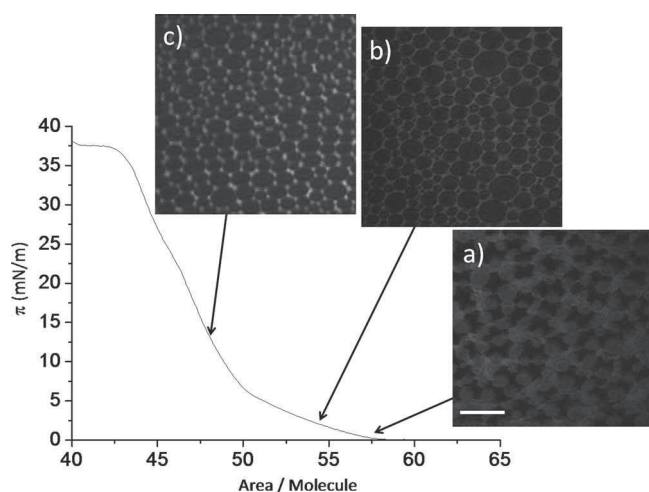


Figure 2. Organization of the mixed monolayer at the air/water interface. Solid curve: Surface-pressure and area isotherm of the MOH/elaidic acid/alkyl-coated Au NPs (20°C); a–c) BAM images recorded at the surface pressures indicated by the arrows. Scale bar: $40 \mu\text{m}$.

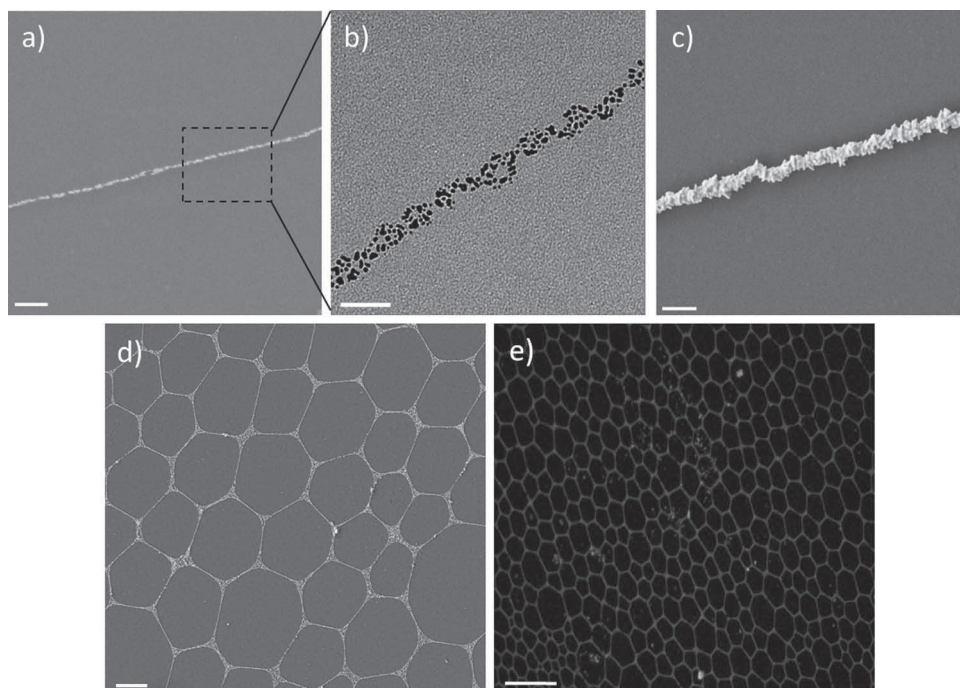


Figure 3. Au nanostructures transferred onto solid substrates. a) SEM image corresponding to a fragment of the Au nanowire network transferred from the air/water interface. Scale bar: 200 nm. b) TEM image corresponding to the indicated region in (a), depicting the individual Au NPs that make up the nanowire. Scale bar: 50 nm. c) SEM image of a fragment of the Au nanowire network following annealing and gold enhancement. Scale bar: 500 nm. d) Wide-area SEM image showing the Au pattern following annealing and gold enhancement. Scale bar: 10 μm . e) Dark field microscopy image showing part of the Au pattern on a transparent glass substrate. Scale bar: 50 μm .

in Figure 3d,e is crucial, since it gives rise to both high transmittance of light (through the empty domains) but also facilitates electronic conductivity (through the gold nanowire network).

The transparency and conductivity profiles of the new self-assembled thin-film gold electrodes are shown in Figure 4. Figure 4a presents a representative UV-vis transmission spectrum of the thin-film gold electrode produced through the surfactant-templated approach. The transmittance values in Figure 4a underscore the remarkable transparency of the gold network; less than 15% of the incoming light was absorbed or scattered upon passage through the film. Importantly, gold enhancement procedures utilizing significantly more concentrated gold seeding solution and/or longer duration of seeding, thus exhibiting thicker gold patterns, had marginal effects upon the film transparency (data not shown).

To characterize the conductivity properties of the new transparent Au nanowire electrodes, we investigated the electrical conductivity profiles in a broad range of distances between electrodes etched on the nanowire film (Figure 4). Such measurements are important for evaluating the practical potential of the new assemblies as conductive electrodes. Figure 4b depicts conductivity measurements carried out by etching upon the Au nanowire network aluminum masks exhibiting different electrode spacings (Figure 4c-d). Importantly, the photolithography procedure followed by Al-selective wet etching^[14] (see Experimental Section) did not damage the gold nanowire network. The current-voltage (I - V) curves in Figure 4b corresponding to three devices prepared through the etching

procedure with significantly different electrode spacings, demonstrate the Au network facilitated electrical conductivity. The average I - V curve in Figure 4b (Figure 2, Supporting Information, shows representative I - V curves from several electrodes), recorded for small- and medium-gap devices (microscopy images in Figure 4c,d, respectively), yielded similar average resistance of a few $\text{k}\Omega \mu\text{m}^{-1}$ (the horizontal line in Figure 4b corresponds to the control electrode current, e.g., without the Au nanowire pattern). This result suggests that contact resistance is the primary parameter affecting the conductivity in these assemblies.

The I - V curve recorded in the long-gap electrode, which is shown in the inset of Figure 4b, indicates that electrical conductivity could still be recorded even when devices exhibiting 1-cm spacings between the electrodes were tested. Optical microscopy images corresponding of the long-range electrode spacing are provided in the Supporting Information, Figure 3). Note that the I - V curve in this electrode configuration does not show Ohmic behavior and the conductivity, while still significant, is four orders of magnitude lower than the small-gap or narrow-gap electrodes. This measurement, however, demonstrates that the newly developed Au nanowire network facilitates electron transport, even on a macroscopic length-scale. Non-linear and low-conductivity characteristics of I - V curves were previously reported.^[15,16] It is assumed that in the centimeter length-scale the transport phenomena will be significantly determined by local defects in the conductive network and/or non-linear hopping-mediated transport phenomena, rather than the contact resistance observed in case of the short-gap and medium-gap electrodes.^[16,17] We

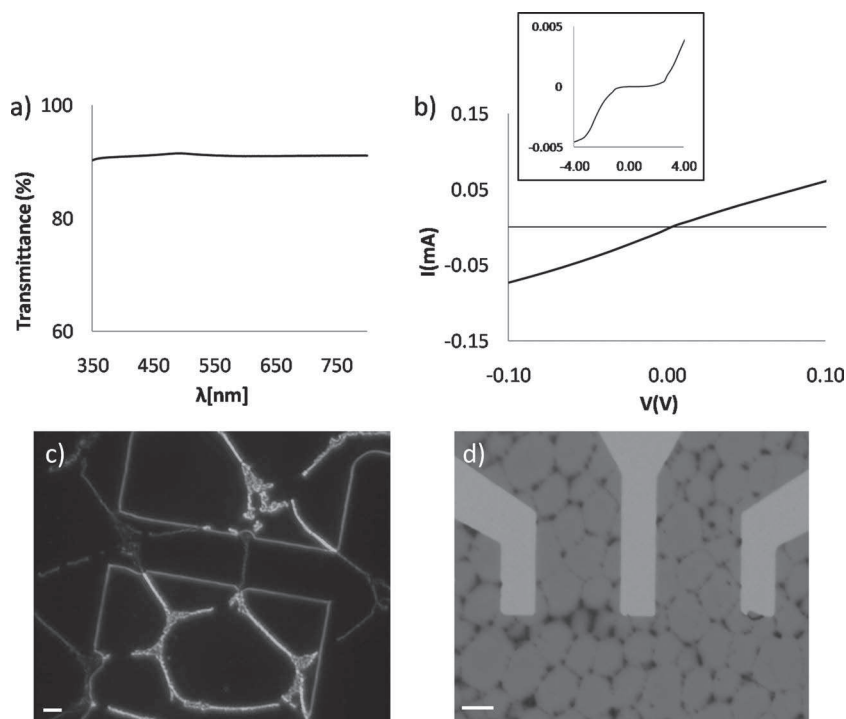


Figure 4. Physical and electrical properties of the patterned Au films. a) Transparency: UV-vis transmittance spectrum demonstrating very high light transparency. b) Conductivity: I - V curves recorded between aluminum electrodes etched onto the Au patterned substrate. Shown are averaged electrical current profiles recorded at different electrode gaps. The I - V curves were recorded for either narrow gaps between electrodes ($3\ \mu\text{m}$) or medium gaps ($50\ \mu\text{m}$). Inset: I - V curve recorded for electrodes exhibiting large gaps ($1\ \text{cm}$). c) Dark-field microscopy image showing a representative short-gap electrode arrangement (parallel bright-field image shown in the Supporting Information file, Figure 1). Scale bar: $1\ \mu\text{m}$. d) Bright-field microscopy image showing a representative medium-gap electrode arrangement. Scale bar: $20\ \mu\text{m}$.

anticipate that the longer-scale conductivity in the new electrode assemblies will be significantly improved through modulation of experimental parameters, including greater nanowire density, reduced defect abundance through more extended annealing and/or gold seeding, adsorption of additional Au nanowire layers (e.g., multilayered assemblies), and others.

In conclusion, we demonstrate a new bottom-up approach for fabrication of transparent conductive electrodes through the use of self-assembled Au NPs patterned at the air/water interface. The experiments indicated that a pattern of alkyl-coated Au NPs can be assembled at the air/water interface through selection of appropriate surfactant molecules co-deposited with the NPs. In the system depicted here we used MOH, which formed condensed circular domains providing a template for assembly of the Au NPs at the grain boundaries, while elaidic acid facilitated uniform distribution of the Au NPs around the condensed domains. Transfer of the Au NP patterns complemented by further enhancement of the gold features through a seeding procedure yielded thin films of interconnected Au nanowire network, exhibiting excellent transparency and conductivity characteristics. The new approach is robust, inexpensive, and amenable to fabrication of TCEs with different areas and electrode spacings.

Experimental Section

HAuCl_4 , tetradecylammonium bromide, sodium borohydride, elaidic acid, MOH, and pentanethiol were purchased from Sigma-Aldrich and used as received. Chloroform (CHCl_3) was HPLC grade (Frutarom Ltd., Haifa, Israel).

Synthesis of the pentanethiol-capped Au NPs was carried out as previously described.^[18] Briefly, a slightly modified Brust procedure,^[19] based upon a two-phase (toluene/water) reduction of HAuCl_4 in the presence of the stabilizing ligand, was used. HAuCl_4 ($100\ \text{mg}$) was dissolved in water ($10\ \text{mL}$) and transferred to toluene ($40\ \text{mL}$) by mixing with tetradecylammonium bromide ($500\ \text{mg}$). Pentanethiol ($6.5\ \mu\text{L}$) was added to the vigorously stirred solution. Finally, NaBH_4 ($200\ \text{mg}$) in water ($1\ \text{mL}$) was added. After $10\ \text{min}$ the solution appeared dark brown, indicating the formation of Au NPs. The solution was further stirred overnight to ensure completion of the reaction. The organic phase was subsequently washed with $2\ \text{M}\ \text{H}_2\text{SO}_4$ and water in a separation funnel and evaporated in vacuum to near dryness. The resultant pentanethiol-capped Au NPs were precipitated by addition of ethanol ($60\ \text{mL}$). After separation by filtration, the precipitate was washed three times with ethanol and dried in vacuo to yield the Au NPs ($34.9\ \text{mg}$) as a black wax, which was easily dissolved in chloroform (final concentration $3.00\ \text{mg}\ \text{mL}^{-1}$). The Au NPs were characterized by TEM and the average diameter of the particles was approximately $3\ \text{nm}$.

All surface-pressure and area isotherms were recorded using a computerized Langmuir trough (model 622/D1, Nima Technology Ltd., Coventry, UK). The surface pressure was monitored using $1\ \text{cm}$ wide filter paper as a Wilhelmy plate. For each isotherm experiment, the desired amount of gold nanoparticles, elaidic acid, and MOH mixture in chloroform (the molar ratio was $1:200:2202$) was spread on the water subphase and equilibrated for $15\ \text{min}$, allowing for solvent evaporation prior to compression. Compression was carried out at a constant barrier speed of $8\ \text{cm}^2\ \text{min}^{-1}$. The average molecule and area values reported in Figure 1 correspond to the total number of molecules: Au NPs, elaidic acid, and MOH. For calculating the Au NP concentration, each Au NP was considered as a single molecule and the molecular weight was calculated based upon the average diameter as determined in a TEM experiment.

A Brewster angle microscope (NFT, Gottingen, Germany) mounted on a Langmuir film balance was used to observe the microscopic structures in situ at the air/water interface. The light source of the BAM was a frequency-doubled Nd:YAG laser with a wavelength of $532\ \text{nm}$ and $20\text{--}70\ \text{mW}$ primary output power in a collimated beam. The BAM images were recorded with a charge coupled device (CCD) camera. The scanner objective was a Nikon superlong working distance objective with a nominal $10\times$ magnification and a diffraction-limited lateral resolution of $2\ \mu\text{m}$. The images were corrected to eliminate side ratio distortion originating from a non-perpendicular line of vision of the microscope.

Hydrophobic coating was carried out as described. A silicon wafer with a thermal oxide layer ($100\ \text{nm} \pm 10\%$, Virginia Semiconductor, Inc, USA) was washed with chloroform and placed in a UV/ozone oven for $30\ \text{min}$. The wafer was subsequently washed with distilled water and placed in a $100\ ^\circ\text{C}$ furnace. Following another UV/ozone oven treatment the silicon wafer was immersed for $1\ \text{h}$ in silane solution (Sigmacote, Sigma) for which heptane was the solvent and subsequently washed with cyclohexane prior to use. Note that the Sigmacote layer was not conductive.

For TEM measurements, films at the desired surface pressures were transferred horizontally onto 400 mesh copper formvar/carbon grids (Electron Microscopy Sciences, Hatfield, PA, USA). TEM images were recorded using a Jeol JEM-1230 transmission electron microscope (JEOL LTD, Tokyo, Japan) operating at 120 kV.

For SEM measurements, films at the desired surface pressures were transferred horizontally onto silicon wafer with a thermal oxide layer: 100 nm \pm 10% (Virginia Semiconductor, Inc, USA). SEM images were recorded using a Jeol JSM-7400F Scanning electron microscope (JEOL LTD, Tokyo, Japan).

The removal of the capping agent following transfer of the monolayer onto solid substrates using the Langmuir–Schaefer (horizontal) method was carried out by placing a glass tube containing the samples in a Thermo Scientific Lindberg Mini-Mite Tube Furnace. An inert environment was achieved by argon flow, which was maintained during the entire heating operation. The samples were heated to 350 °C for 35 min. It was found that in the absence of the heat treatment the seeding procedure could not be carried out, and, furthermore, no conductivity was established. This observation indicates that the capping agents were indeed removed because the seeding protocol requires the presence of exposed gold surfaces to catalyze the reduction and deposition of the gold structures. Overall, the experimental conditions (temperature, duration, insert atmosphere) were determined through trial and error, designed to remove as effectively as possible the organic moieties as well as to prevent oxidation.

Gold enhancement (seeding) was accomplished by dissolving HAuCl₄ (20 mg) in water (1 mL), which was added to a KSCN solution (1 mL, 60 mg mL⁻¹). The precipitate formed was separated from the solution using a centrifuge (4000 g) and added to a 8 mL of 1 M buffer solution of phosphoric acid (pH 5.5). A solution of hydroquinone (1 mL, 5.5 mg mL⁻¹), which constituted the reducing agent, was added to the buffer solution. The Au NP pattern transferred onto the solid substrate was then immersed for 3 min immediately after adding the hydroquinone.

Aluminum electrodes were prepared as follows. First, 50 nm of aluminum film was deposited on the Au patterns using electron beam evaporation. Following the deposition, the electrodes structures were defined using photolithography and Al wet etching.^[14] Finally, the photoresists used for the electrode definition process were removed using oxygen plasma. Optical microscopy, SEM, and energy dispersive X-ray spectroscopy (EDS) revealed that no damage to the Au-network was done during this process and no traces of Al were found inside the gap. Three gap sizes were fabricated with three different lengths: 3 μ m, 50 μ m, and 1 cm (see Figure 4 and Supporting information). Room temperature electrical measurements were carried out in a two-probe configuration using a probe-station equipped with a Keithley 4200SCS semiconductor parameter analyzer.

Supporting Information

Supporting Information is available from the Wiley Online Library or from the author.

Acknowledgements

The authors are grateful to Dr. T. Mokari for help with organic capping agent removal protocols and Itzik Kalifa and Netta Hendler for help with electrode preparations and conductivity measurements.

Received: April 6, 2011

Revised: June 16, 2011

Published online: August 16, 2011

- [1] A. Kumar, C. Zhou, *ACS Nano* **2010**, *4*, 11.
- [2] P. Calandra, G. Calogero, A. Sinopoli, P. G. Gucciardi, *Int. J. Photoenergy* **2010**, *2010*, 1.
- [3] G. M. Wallraff, W. D. Hinsberg, *Chem. Rev.* **1999**, *99*, 1801.
- [4] W. Lu, C. M. Lieber, *Nat. Mater.* **2007**, *6*, 841.
- [5] R. Volinsky, R. Jelinek, *Angew. Chem Int. Ed.* **2009**, *48*, 4540.
- [6] A. R. Tao, J. Huang, P. Yang, *Acc. Chem. Res.* **2008**, *41*, 1662.
- [7] N. Markovich, R. Volinsky, R. Jelinek, *J. Am. Chem. Soc.* **2009**, *131*, 2430.
- [8] C. R. Hansen, F. Westerlund, K. Moth-Poulsen, R. Ravindranath, S. Valiyaveetil, T. Bjørnholm, *Langmuir* **2008**, *24*, 3905.
- [9] T. Hassenkam, K. Nørgaard, L. Iversen, C. J. Kiely, M. Brust, T. Bjørnholm, *Adv. Mater.* **2002**, *14*, 1126.
- [10] D. Vollhardt, *Langmuir* **2002**, *18*, 6571.
- [11] S. Meltzer, *Langmuir* **2001**, *17*, 1713.
- [12] L. Hu, H. S. Kim, J.-Y. Lee, P. Peumans, Y. Cui, *ACS Nano* **2010**, *4*, 2955.
- [13] D. Vollhardt, V. B. Fainerman, *Adv. Colloid Interface Sci.* **2010**, *154*, 1.
- [14] K. R. Williams, K. Gupta, M. Wasilik, *J. Microelectromech. Sys.* **2003**, *12*, 761.
- [15] D. Azulai, T. Belenkova, H. Gilon, Z. Barkay, G. Markovich, *Nano Lett.* **2009**, *9*, 4246.
- [16] T. Ogawa, *Thin Solid Films* **2001**, *393*, 374.
- [17] A. Bezryadin, C. Dekker, G. Schmid, *Appl. Phys. Lett.* **1997**, *71*, 1273.
- [18] M. Brust, M. Walker, D. Bethell, D.J. Schiffrin, R. Whyman, *J. Chem. Soc. Chem. Commun.* **1994**, 801.
- [19] K. Nørgaard, M. J. Weygand, K. Kjaer, M. Brust, T. Bjørnholm, *Faraday Discuss.* **2004**, *125*, 221.